Novel Polymorph of GaSe

Justyna Grzonka,* Marcel S. Claro, Alejandro Molina-Sánchez, Sascha Sadewasser, and Paulo J. Ferreira

2D GaSe is a semiconductor belonging to the group of post-transition metal chalcogenides with great potential for advanced optoelectronic applications. The weak interlayer interaction in multilayer 2D materials allows the formation of several polymorphs. Here, the first structural observation of a new GaSe polymorph is reported, characterized by a distinct atomic configuration with a centrosymmetric monolayer (D_{3d} point group). The atomic structure of this new GaSe polymorph is determined by aberration-corrected scanning transmission electron microscopy. Density-functional theory calculations verify the structural stability of this polymorph. Furthermore, the band structure and Raman intensities are calculated, predicting slight differences to the currently known polymorphs. In addition, the occurrence of layer rotations, interlayer relative orientations, as well as translation shear faults is discussed. The experimental confirmation of the new GaSe polymorph indicates the importance of investigating changes in the crystal structure, which can further impact the properties of this family of compounds.

J. Grzonka, M. S. Claro, A. Molina-Sánchez, S. Sadewasser, P. J. Ferreira
INL-International Iberian Nanotechnology Laboratory
Av. Mestre José Veiga s/n, Braga 4715-330, Portugal
E-mail: justyna.grzonka@gm.uca.es

J. Grzonka
Faculty of Sciences
Cadiz University
Campus Rio San Pedro, Puerto Real, Cadiz 11510, Spain

A. Molina-Sánchez
Institute of Materials Science (ICMUV)
University of Valencia
Catedrático Beltrán 2, Valencia E-46980, Spain

S. Sadewasser
QuantaLab
Braga 4715-330, Portugal

P. J. Ferreira
Materials Science and Engineering Program
The University of Texas at Austin
Austin, TX 78712, USA

P. J. Ferreira
Mechanical Engineering Department and IDMEC
Instituto Superior Técnico
University of Lisbon
Av. Rovisco Pais, Lisboa 1049-001, Portugal

1. Introduction

2D layered materials and their superior properties offer a platform that allows the formation of heterostructures capable of producing devices with enhanced functionalities.[1] In this regard, although most research on heterostructures has focused on 2D transition metal dichalcogenides (TMD), more recently 2D metal mono-chalcogenides have attracted increasing interest. It has been shown that these post-transition metal chalcogenides (PTMC) have very different electronic and optoelectronic properties, when compared with TMDs. For instance, in contrast to most TMDs, GaSe possesses a direct bandgap in the visible region of spectra in bulk form. Yet, when reduced to a monolayer, the transition to a quasi-direct bandgap is observed.[2,3] The band structure of a GaSe monolayer exhibits the typical "Mexican hat" dispersion[2,4,5] at the top of the valence band, leading to a high density of states, which has several applications in thermoelectrics[6] and the emerging field of spintronics.[7–9] It has been reported[3,10] that the bandgap of 2D PTMCs increases considerably when decreasing the thickness from bulk to a few-layers' configuration, covering the whole visible region.[11,12] As with most 2D materials, the layer stacking sequence may crucially affect the properties. Therefore, it is essential to understand and control the atomic structure, the interlayer relative orientations and the stacking sequence.

The compound Ga—Se belongs to the group of layered III-VI binary chalcogenide semiconductors and can exist in various phases and stoichiometries, that is, GaSe and Ga_2Se_3.[13] GaSe, the focus of the present study, crystallizes in a hexagonal-type structure. Each of its layers has a honeycomb-type lattice and contains four monoatomic sheets—two layers of Ga sandwiched between two layers of Se—known as tetralayers (TL). Each Ga atom is covalently bound to three equally distant neighboring Se atoms and another Ga atom, which is again bound to three further Se atoms. There are no dangling bonds in this system, and the individual TLs are bonded together by weak van der Waals (vdW) interactions across an interlayer distance of ≈8 Å.[14] This weak interlayer interaction allows the formation of several polymorphs.

Polymorphism in the context of crystallography is the occurrence of different crystal structures for the same chemical entity.[15] In other words, a specific composition can form different crystal structures of entirely different symmetry and periodicity.[16] A special form of polymorphism is polytypism, which applies to closed-packed or layered materials, where polytypes

Figure 1. Schematic illustrations of the a) β, b) ε, c) δ, d) γ polytypes, and new e) γ' polymorph of bulk GaSe. The yellow arrows indicate the position of van der Waals (vdW) gaps. Unit cells are shown by grey rectangles, the dashed red lines show the different geometric patterns and layer alignments.

are characterized by constituent layers with identical structures but different periodicities perpendicular to the layer plane (i.e., different stacking sequences).[16] The well-known polytypes of GaSe are named as ε-(2R), β-(2H), γ-(3R), and δ-(4H), based on different stacking sequences between the adjacent layers (**Figure 1**a–d). Despite the similarities in band structure,[17] the electronic and optical properties show particularities due to the presence or lack of symmetry. In particular, differences are expected mainly in properties related to the spin and interaction with polarized light,[18] where the crystal symmetry defines degenerate states and transition selection rules.

All of the polytypes mentioned above have unit cells which are similar along the [0001] orientation, but differ in the number and lateral placement of the stacked TL. These are obtained either by rotation and/or translation operations, namely a 180° rotation and translation of 1/3 or 2/3 of the unit cell along the <1010> type directions.[19] For the β-polytype (P6$_3$/mmc space group), the adjacent layers are rotated by 180° and stacked directly upon one another, thus referred to as AA′-type stacking. The ε-polytype (P-6m2 space group) lacks an inversion center, so the stacking is accomplished through translation of the unit cell by 2/3 and 1/3 along the <1010> type directions in alternating layers, and referred to as AB-type stacking.[20] In the case of the γ-polytype (R3m space group), the stacking is accomplished through the translation of the unit cell by 1/3 along the <1010> type directions. The γ-polytype is similar to 3R stacking, which follows a pattern of the type ABCABC. The δ-polytype (P6$_3$mc space group) consists of a four-layer structure with an ACABA sequence. The most reported GaSe polytypes in the literature are the ε and γ types.[13,21–25] However, it was observed that polytypes frequently depend on the growth conditions and methods utilized.[26,27] Due to its importance, the stability, formation energy, and band structure of known polytypes has been extensively studied by ab-initio methods.[17,28] According

to these most recent reports, the formation energies are close enough to expect the coexistence of most of the stacking variations, leading to a high amount of stacking faults.

In this paper, we provide direct observation of these polytypes and their defects, in samples grown by molecular beam epitaxy (MBE). The work provides experimental data that can be correlated with previous theoretical studies, as well as will allow future research to improve methodologies for crystal growth. Furthermore, it has been shown that many 2D materials possess different structures of the monolayer, such as trigonal prismatic and octahedral monolayers of MoS$_2$ belonging to the TMDs.[29,30] For the PTMC InSe, a new polymorph with a centrosymmetric TL (cs-TL) (point group D$_{3d}$) was recently predicted by first-principles calculations, in addition to the experimentally known non-centrosymmetric TL (ncs-TL) of point group D$_{3h}$.[31] This new InSe polymorph was predicted, theoretically, to exhibit enhanced electronic properties, that is, wider optical spectral response and larger electron mobility, and thermodynamic and kinetic stability. In addition, while the current work was carried out, the same polymorph was predicted in GaSe.[32] Due to the close similarity between InSe and GaSe, one can also speculate an enhancement of the GaSe electronic properties. Yet, despite the predictions that both PTMC polymorphs are stable, their experimental observation has not been reported so far, and thus their properties are still unknown.

Here, we report the direct observation of a new GaSe polymorph, experimentally obtained by MBE growth, with a cs-TL (D$_{3d}$), and a γ-GaSe type stacking, which we define as γ'-GaSe (Figure 1e). It is distinct from the well-known polymorphs based on ncs-TLs (D$_{3h}$) that lack inversion symmetry. In this regard, we show a comprehensive characterization of the atomic-scale crystal structure of this and other GaSe polymorphs by scanning transmission electron microscopy (STEM), including the nature of stacking order and defects. The stability of this new

polymorph is verified by density functional theory (DFT) calculations, from which also the band structure and Raman intensities are predicted.

2. Results and Discussion

2.1. GaSe Growth on Si (111) and Sapphire (0001)

The growth of GaSe films was performed by MBE on Si (111) and sapphire (0001) substrates. The growth conditions were determined based on several experiments where a proper balance of Ga and Se fluxes impinging the surface during growth was accomplished. The III–VI ratio was precisely controlled by the Se cracker valve aperture and the Ga Knudsen cell temperature, following a similar procedure reported by Lee et al.[13] The optimized substrate temperature during the growth was determined to be 550 °C, for which the lowest value of surface roughness was obtained within the 450–600 °C range. The evolution of the phases during growth was primarily monitored by in-situ reflection high energy electron diffraction (RHEED), as shown in **Figure 2**a. After growth, the phase purity was investigated by X-ray diffraction (XRD) (Figure 2c) and Raman spectroscopy (Figure 2d), which are highly sensitive in detecting a mixture of phases, even when they are not visible in RHEED. The Raman spectrum shows peaks at 132, 205, and 307 cm^{-1}, corresponding to the A^1_{1g}, E^1_{2g}, and A^2_{1g} vibration modes of GaSe, respectively.[13] The presence of the Ga_2Se_3 phase was not detected. Furthermore, the distinct and narrow peaks in the XRD and Raman spectra support the high quality of the films. The surface topography obtained by atomic force microscopy (AFM) exhibits surface roughness of 1 to 2 nm after 90 nm of GaSe growth (Figure 2b), in fact the best results obtained so far for this material.[13]

2.2. Basic γ-GaSe Structure

To further investigate the crystal structure of our GaSe layers, advanced X-ray methods and aberration-corrected high-angle annular dark-field (HAADF) STEM were applied. From the $(11\bar{2}0)$ peak at $2\theta = 48.34°$ obtained by grazing-incidence in-plane X-ray diffraction (GIIXRD) (**Figure 3**a), the lattice parameters $c = 15.916(7)$ Å and $a = b = 3.762(176)$ Å were obtained, which correspond to previous experimental and theoretical reports for this material. The φ-scan of this peak (Figure 3b) can be used to understand the epitaxial (crystallographic) relationship between the GaSe and both substrates. The sample grown on sapphire shows that although it is preferentially aligned to the substrate (GaSe (110)∥sapphire (110)), the layers are twisted within a wide distribution of angles, as shown by the broadness of the peak. Consequently, the growth of the film at the onset is not well aligned with the substrate orientation, indicating that the GaSe layers are weakly bound to the sapphire substrate.
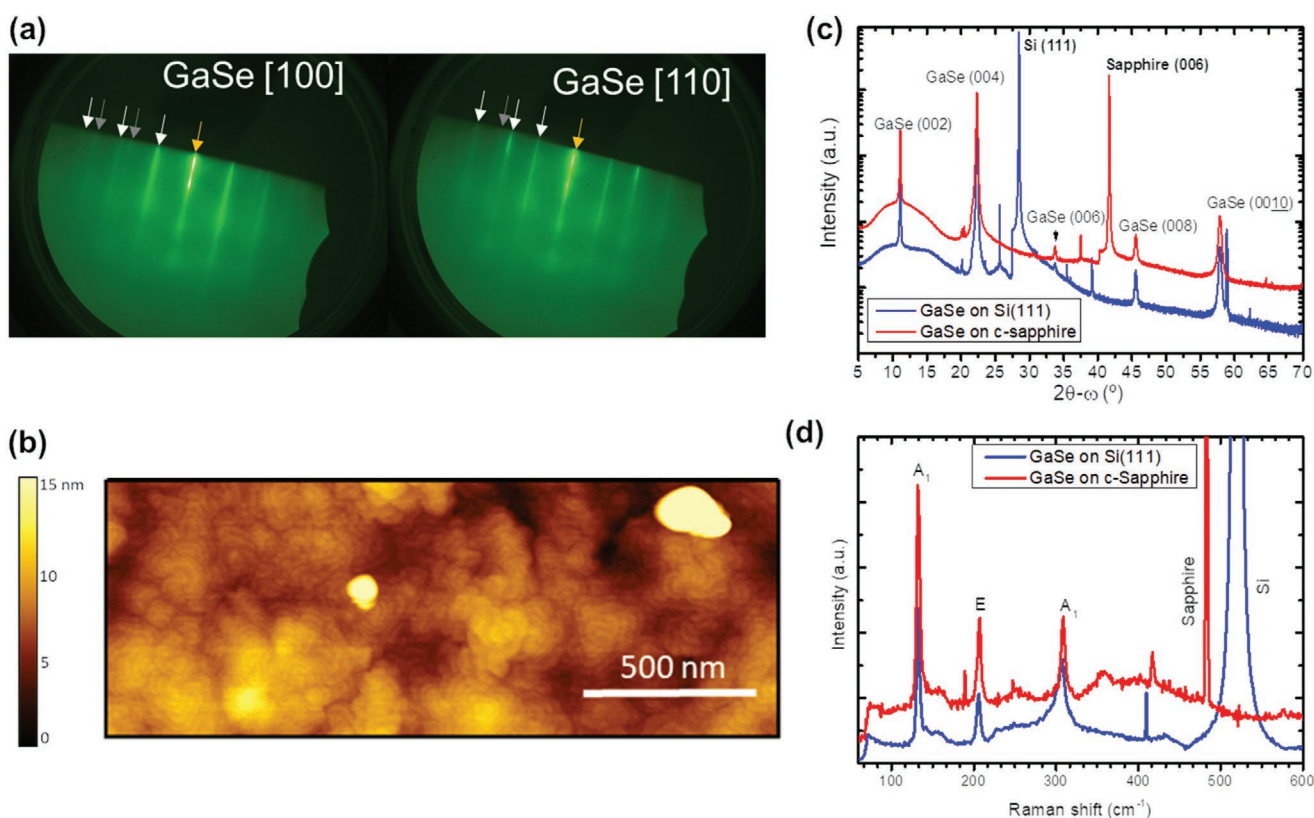

Figure 2. a) Reflection high-energy electron diffraction (RHEED) acquired during the growth of GaSe on c-sapphire. b) AFM image of a 90 nm thick GaSe film grown on a Si (111) substrate. c) XRD and d) Raman spectra of GaSe films grown on Si (111) and c-sapphire.
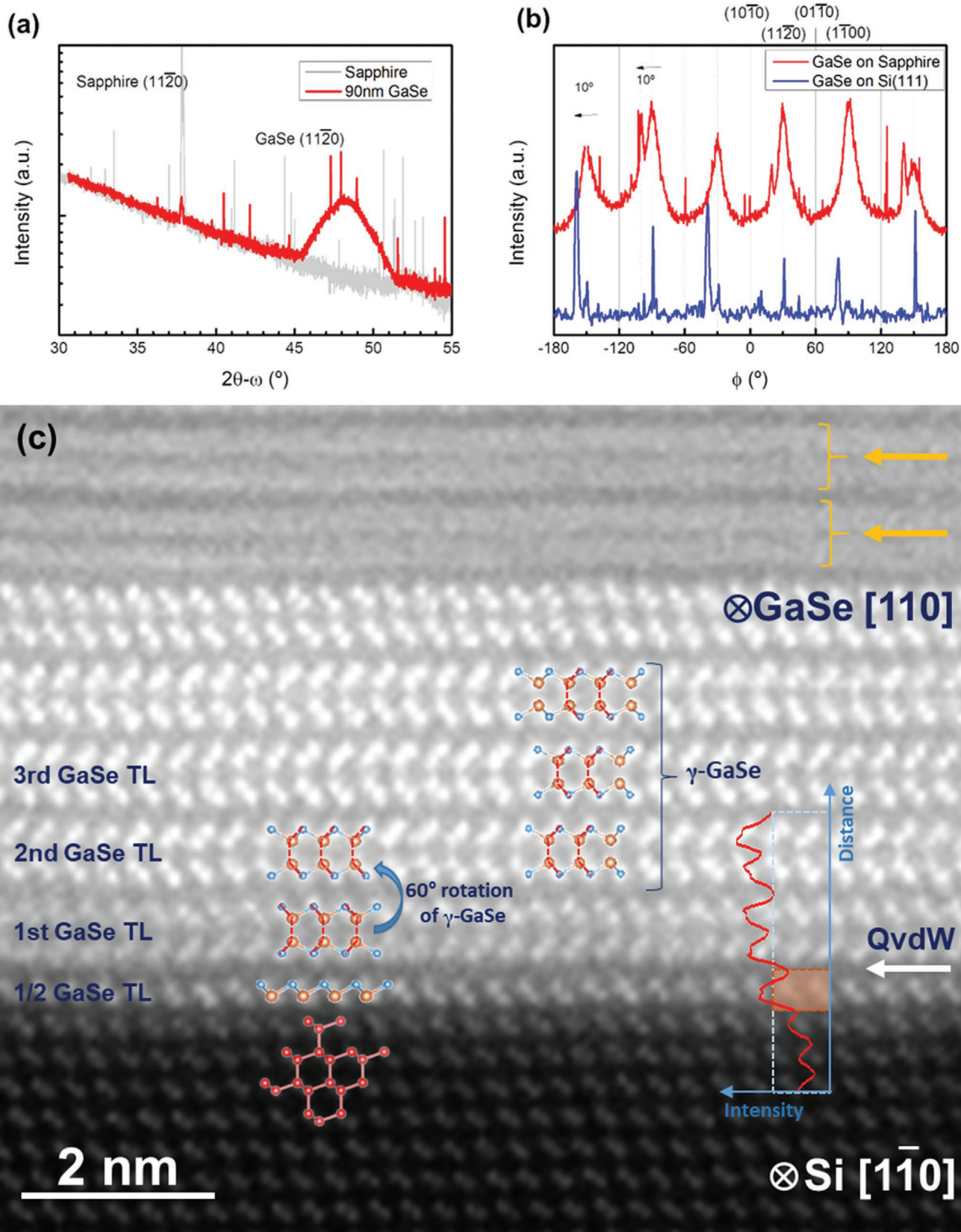
Figure 3. a) Grazing-incidence in-plane X-ray diffraction (GIIXRD) of 90 nm GaSe on *c*-sapphire and b) *φ*-scan of the (11$\bar{2}$0) GaSe peak on *c*-sapphire and Si substrates. c) HAADF-STEM image across the interfacial region between the Si substrate and the GaSe film with overlaid structural models of Si

ADVANCED
SCIENCE NEWS
www.advancedsciencenews.com

ADVANCED
FUNCTIONAL
MATERIALS
www.afm-journal.de

Thus, defects are expected to appear, due to the random orientation of the starting layer and subsequent layers. On Si (111) substrates, the peaks are narrower, indicating that the crystalline quality and epitaxial growth improve. Furthermore, extra peaks in the φ-scan (Figure 3b), shifted from the main peaks of (GaSe (110)‖sapphire (110)), were found. In particular, a misalignment of ≈10° was observed in the GaSe films grown on both substrates. This has also been observed by[33] where ≈50% of the monolayer GaSe domains was oriented with a 10.5° interlayer rotation with respect to the underlying graphene. The authors have shown that a 10.9° interlayer rotation is energetically preferred in GaSe/graphene heterostructures. In our case, since the φ-scan refers to a signal coming from several layers, it indicates that the twist of 10° may also by favorable between the GaSe layers in the stack, and not only with respect to the substrate.

Along the [110] crystallographic orientation, the Se and Ga atomic columns are entirely separate, which allows us to distinguish between the various polytypes due to their distinct atomic arrangements. In the GaSe films two polytypes were detected, in particular γ-GaSe (Figure 3c) and β-GaSe (Figure S1, Supporting Information), where the latter is present in much less amounts. These polytypes are confirmed by the structural models overlaid on the experimental images. In Figure 3c a close view of the interfacial region between the GaSe vdW layers and the Si (111) substrate is shown. The layers are well ordered at the initial stage of growth, as shown by the clearly visible structure close to the substrate, including the vdW gaps separating the TLs. The upper two TL shown by the yellow arrows do not exhibit sharp contrast due to an in-plane rotation of the layers. The reason for the rotation of the layers is most likely the weak vdW bonding. The contrast between Ga and Se columns is low, due to their similar atomic numbers ($Z_{Ga} = 31$, $Z_{Se} = 34$).

At the interface between the Si (111) substrate and the GaSe film a "quasi-van der Waals gap"[34] is present (white arrow), suggesting that the dangling bonds at the surface of the substrate are terminated. This passivation is demonstrated by the integrated intensity profile across the interfacial region (red line), which shows a significant increase in intensity for the first two atomic layers adjacent to the Si substrate, suggesting a higher average atomic number. This layer corresponds well to the presence of half of a TL also known as a Ga—Se half-sheet termination layer.[35] This Ga—Se termination layer (1/2 GaSe TL in Figure 3c) has a structure identical to a Se—Ga—Ga—Se TL cut in half at the Ga—Ga bond. Therefore, the Ga—Se half-sheet termination layer should provide an ideal passivation for the Si (111) surface, which is expected to be stable also as a substrate for subsequent layer growth.

In addition to the passivation layer, a rotation of 60° between the first and second layer is observed (Figure 3c). A similar phenomenon was reported for the growth of ε-GaSe on a GaN substrate.[13] In this report, the first GaSe layer was rotated 60°

relative to the layers deposited on top and the initial two TLs were considered as β-GaSe polytype however, the subsequent layers were stacked as pure ε polytype. This behavior was attributed to the fact that the ε-polytype exhibits a higher energy stability than the β-polytype. However, in our film, the 60° rotation of the γ-GaSe TL does not lead to the formation of a β-GaSe polytype (Figure 3c and Figure S1, Supporting Information). Instead the atomic model of the 60° rotated γ-GaSe structure matches well with the experimental image in Figure 3c. The discrepancy between the overlaid atomic model of GaSe and the experimental atomic positions obtained by HAADF-STEM shows that the vdW film is not well aligned with the underneath Ga—Se passivation layer on the Si surface. Such a deviation has been attributed to the creation of a translational shear fault (TSF),[36] wherein the TLs stacking in γ-GaSe is not preserved.

2.2.1. New GaSe Polymorph—Atomic Structure and Ab-Initio Calculations

In addition to regions where the γ-GaSe polytype with ncs-TLs is present, we also observed regions which exhibit an atomic structure not covered by any of the known polytypes described in Figure 1a–d (β, ε, δ, γ). This new atomic arrangement is shown in **Figure 4** and is based on cs-TLs of GaSe. In the typical configuration of an individual Se—Ga—Ga—Se TL observed along the [110] zone axis, Ga atoms sit on top of each other, and the Se atoms are aligned, creating nonparallel Se—Ga dumbbells (Figure 4a, top). However, in the new arrangement, the Ga atoms keep the same positions, while the Se atoms of one half-layer change their positions to create a parallel dumbbell configuration, for which the atomic model is presented in Figure 4b. This polymorph is centrosymmetric with point group D_{3d}. As the stacking sequence in this new arrangement (Figure 4c) is similar to γ-GaSe, we define it as a new polymorph γ'-GaSe. The fast fourier transformation (FFT) of the γ'-GaSe indicates a rhombohedral structure, which is identical to the γ-GaSe phase (Figure 4d). The series of closely spaced satellite spots in the FFT close to the (000), (003), (01$\bar{1}$), and (01$\bar{4}$) reflections corresponds to the lattice parameter of the superlattice, allowing us to determine the periodicity of the structure, which is related with the layered vdW nature of the film.

We propose that the reason for the formation of the cs-TL of GaSe is the 60° rotation of half of the GaSe TL with respect to the other half. In Figure 4a (bottom), the 60° rotation of the upper triple metal-chalcogen bonds is illustrated, which leads to the parallel dumbbell configuration characteristic of the cs-TL of GaSe observed in our films. We believe that it is caused by the layer-by-layer and out-of-equilibrium MBE epitaxial growth. In other words, if the growth occurs layer-by-layer, both configurations of TLs (cs-TL and ncs-TL, corresponding to parallel and non-parallel Se—Ga dumbbells configurations, Figure 4a)

(represented by red circles) along the [1$\bar{1}$0] zone axis and γ-GaSe polytype (represented by Ga (orange) and Se (blue) circles) along the [110] zone axis. The yellow arrows indicate rotated GaSe TL and the white arrow shows a quasi-van der Waals gap (QvdW) between the passivated Si (111) substrate and the GaSe film. An intensity profile across the interface shows higher intensity for the top two atomic layers of the substrate (highlighted orange area of the profile) when compared with Si, which confirms the passivation process with a half GaSe TL as part of the growth process. A 60° rotation of the first full GaSe TL with respect to the subsequent TLs is also observed.
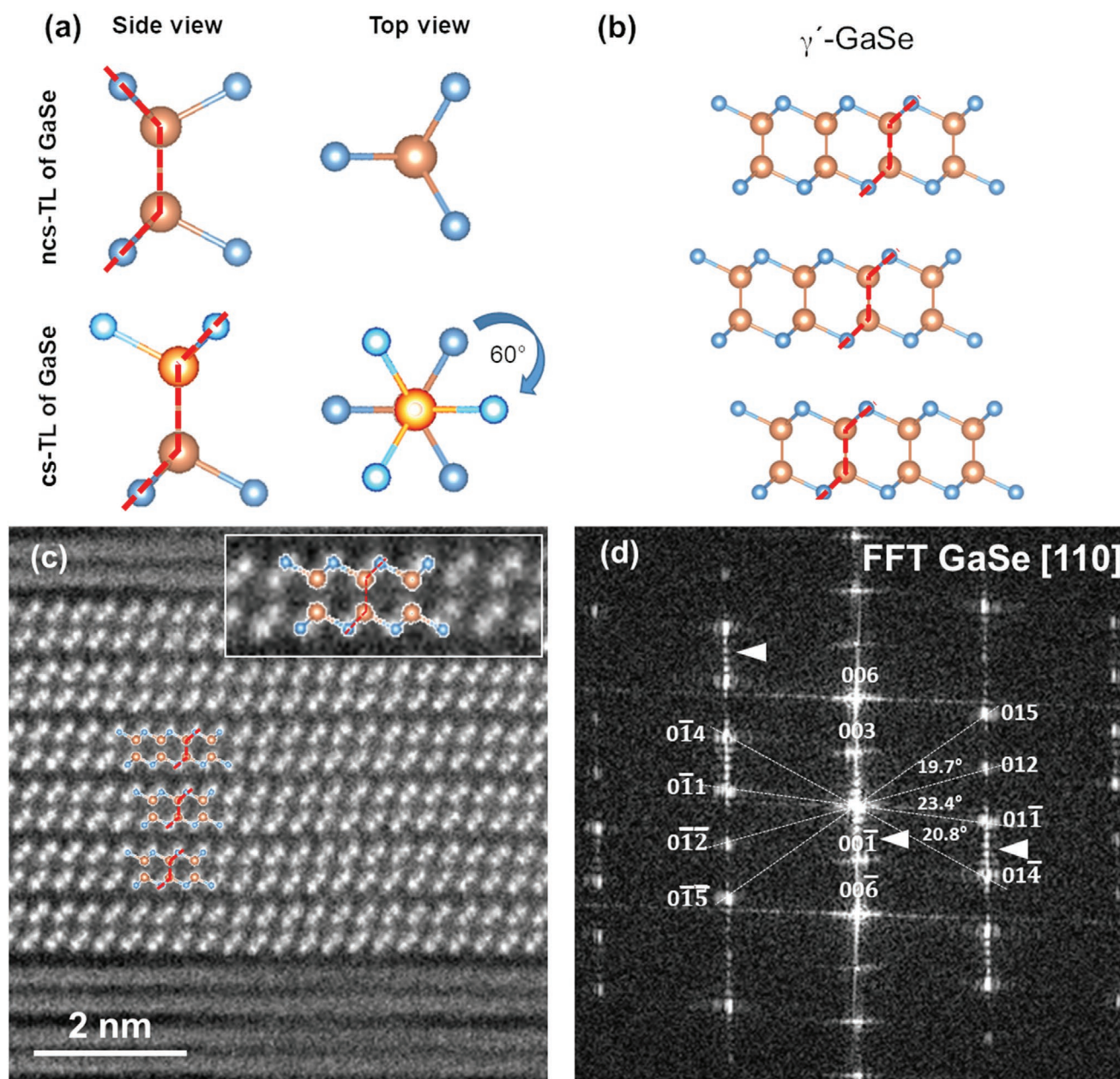
2104965 (5 of 11)

ADVANCED
SCIENCE NEWS
www.advancedsciencenews.com

**ADVANCED
FUNCTIONAL
MATERIALS**
www.afm-journal.de

Figure 4. a) Schematic illustration of the Se3—Ga—Ga—Se3 unit showing both the side and top views of the triple Ga—Se bonds for regular ncs-TL of GaSe (top) and the new cs-TL of GaSe (bottom). In the cs-TL one half of the TL is rotated by 60° with respect to the other half. b) Atomic model of the new γ'-GaSe polymorph. c) HAADF-STEM image of the new γ'-GaSe polymorph, consisting of centrosymmetric TL with different atomic arrangement of the Se atoms compared with the already described ncs-TL polymorph. The inset is showing the higher magnification of the HAADF-STEM together with an overlaid model. d) FFT of the image in (c) indicating the presence of a rhombohedral GaSe phase. The superlattice reflections (white arrows) indicate a large lattice parameter.

can nucleate as a new island, as the Ga—Ga bond is free to rotate around the bond axis.

To evaluate the stability of the γ'-GaSe versus the γ-GaSe, ab-initio calculations were performed. The unit cell of both phases has 12 atoms and point group symmetry C_{3v}. However, the new centrosymmetric GaSe TL polymorph has a D_{3d} point group, which is different from point group D_{3h} for the non-centrosymmetric GaSe TL polymorph. The difference in total energy is less than 0.01 Ry, which indicates that both phases can

coexist, supporting the above proposed nucleation hypothesis. We have verified that the phonon modes of both structures are positive, which assures the stability of both phases. This indicates that, once a full TL is formed in a chosen configuration, an energy barrier needs to be surpassed in order to convert the TL into the other polymorph. Moreover, the interlayer distance between TLs is practically identical in both polymorphs with a value in both cases of ≈4.83 Å. In this context, **Figure 5**a,b shows the band structure of both phases. The band structures
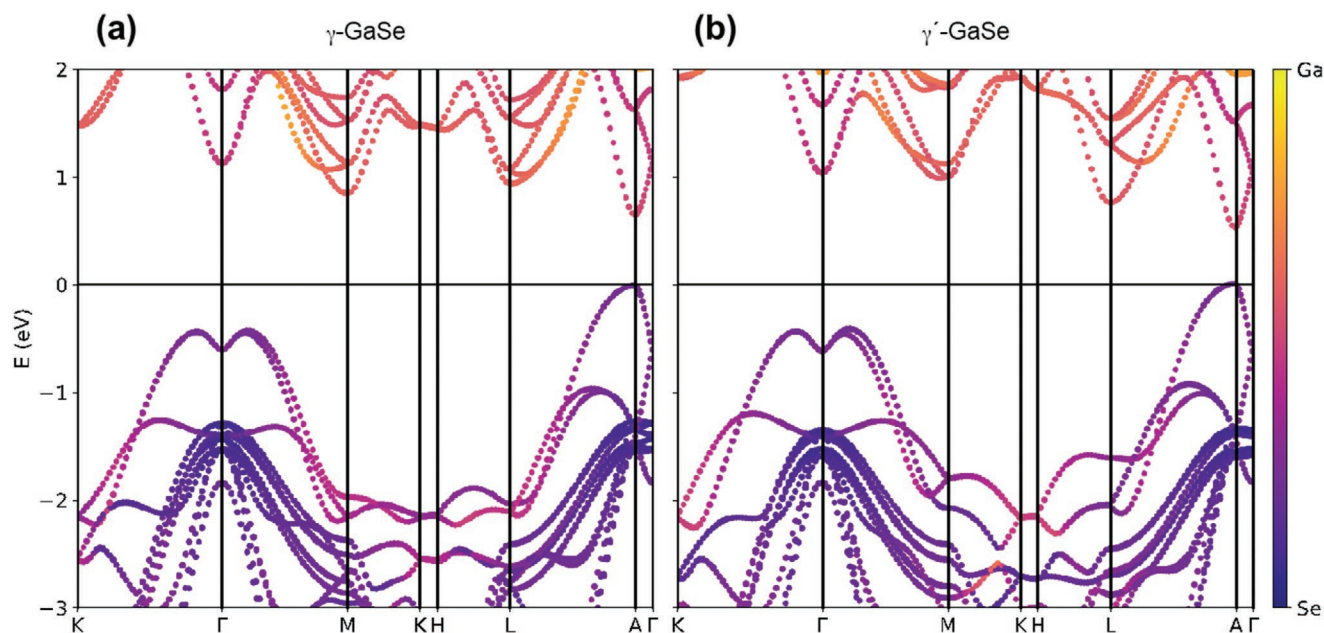
Figure 5. Band structures of a) γ-GaSe and b) γ'-GaSe polymorphs. The color map represents the sum of the weights of s, p_x, p_y, and p_z atomic orbitals of Ga and Se.

around Gamma exhibit the well-known Mexican-hat of gallium and indium chalcogenides.[10] The only differences are in points of the Brillouin zone of smaller symmetry, for example around the M and K points, in which some degeneracies are broken. The calculated bandgap of γ-GaSe and γ'-GaSe is placed at the point A of the Brillouin zone, analogously to InSe.[37] Bandgaps are 0.648 and 0.523 eV for γ-GaSe and γ'-GaSe, respectively. In general, our results independently corroborate recent calculations of Nitta et al.[32] Yet, the difference in the bandgap can be smaller due to the lattice matching of both phases as a result of the growth process. We have also calculated the γ-phase with a rotation of one layer of 60° (see band structure in Figures S2 and S3, Supporting Information). In this case the bandgap is also very similar to that obtained for the γ and γ' phases. We have also represented in the band structure the weight of the atomic orbitals of Ga and Se atoms (sum of the contribution of s, p_x, p_y, and p_z for each atom). The weight of the atomic projections is practically identical for the γ and γ' phases. In both phases the atomic composition of the valence band states is at great extent dominated by Se atomic orbitals. On the other side, the conduction band states, in particular at the bandgap, exhibit a stronger hybridization of Ga and Se orbitals than the valence band states. It is also worth to mention that DFT inherently underestimates the bandgap. More precise calculations of the bandgap would require the GW method to account for the electronic correlation and Bethe–Salpeter for accounting the electron–hole coulomb interaction.[38] Nevertheless, DFT is sufficiently accurate for the study of structural and vibrational properties. The use of GW-BSE approaches is suitable for optical properties, out of the scope of this work. Regarding the calculation of the phonon frequencies and Raman intensities of the three polymorphs (see **Figure 6**a and Figure S4, Supporting Information), also some differences are found. For the Raman peak A_1, the peak of higher intensity, the calculated frequencies

are very similar. For the phonon mode E, our calculations predict a frequency difference of 6 cm^{-1}. The phonon modes A_1 at higher energy (at 300 cm^{-1}) are also very similar. Therefore, identification of distinct polymorphs by optical spectroscopy (i.e., photoluminescence or Raman spectroscopy) is expected to be very challenging, in particular if we consider the minor differences observed in the band structures and Raman spectra. We have also included in Figure 6b the atomic displacements in the TL of each Raman active phonon. The pattern of the atomic displacements is the same for the three phases, with only slight differences in the amplitude of the displacement. This explains the challenging task of identifying different phases using Raman spectroscopy. Our samples, which consist of mixed polymorphs do not display visible differences, due to the broadness of the Raman and XRD spectra.

In the present work, the new γ'-GaSe polymorph based on cs-TLs of GaSe is located close to the substrate, as well as across the entire film thickness. In a previous report,[39] only a single cs-TL was observed near a Ge (111) substrate. For this individual GaSe cs-TL, the authors confirmed by electron-energy loss spectroscopy that the two Ga columns were located between the Se columns, and it was speculated that this individual TL is of metastable nature.[39] In **Figure 7**a, a HAADF-STEM image of the γ'-GaSe phase grown on top of two TL of γ/ε-GaSe polytypes is shown. Note that for γ-GaSe and ε-GaSe the first two TL are identically stacked, while the third TL is the only one that differs, as shown in Figure 1b,d. The atomic model showing the stacking of the experimental TLs (Figure 7a) indicates that the γ'-GaSe stacking follows the same stacking sequence as the γ-GaSe

Furthermore, we also observed a configuration in which new cs-TLs alternate with conventional ncs-TL layer by layer (**Figure 8**a). For this mixture of polymorphs (see atomic model in Figure 8b), the stacking of the first three TLs matches that
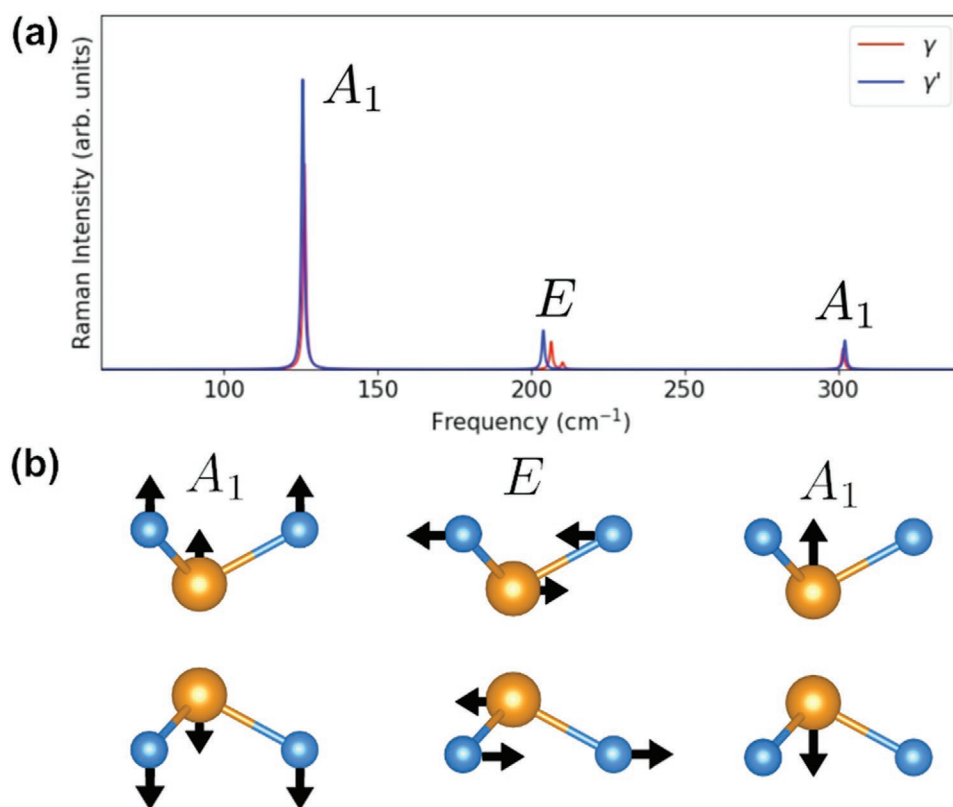
**ADVANCED
SCIENCE NEWS**
www.advancedsciencenews.com

**ADVANCED
FUNCTIONAL
MATERIALS**
www.afm-journal.de

Figure 6. a) Raman intensities and phonon modes of γ-GaSe (red) and γ'-GaSe phases (blue). b) The atomic displacements of each Raman active phonon mode are shown for one TL.

of the ε-GaSe polytype, although the middle layer exhibits the atomic arrangement of the cs-TL, while the surrounding TLs exhibit a ncs-TL type polymorph. Between the 3rd and 4th GaSe TLs, a TSF is observed. The atomic configuration in the 4th GaSe TL is a mirror reflection of the 2nd GaSe TL (both cs-TLs). We have also found another defect which consists of
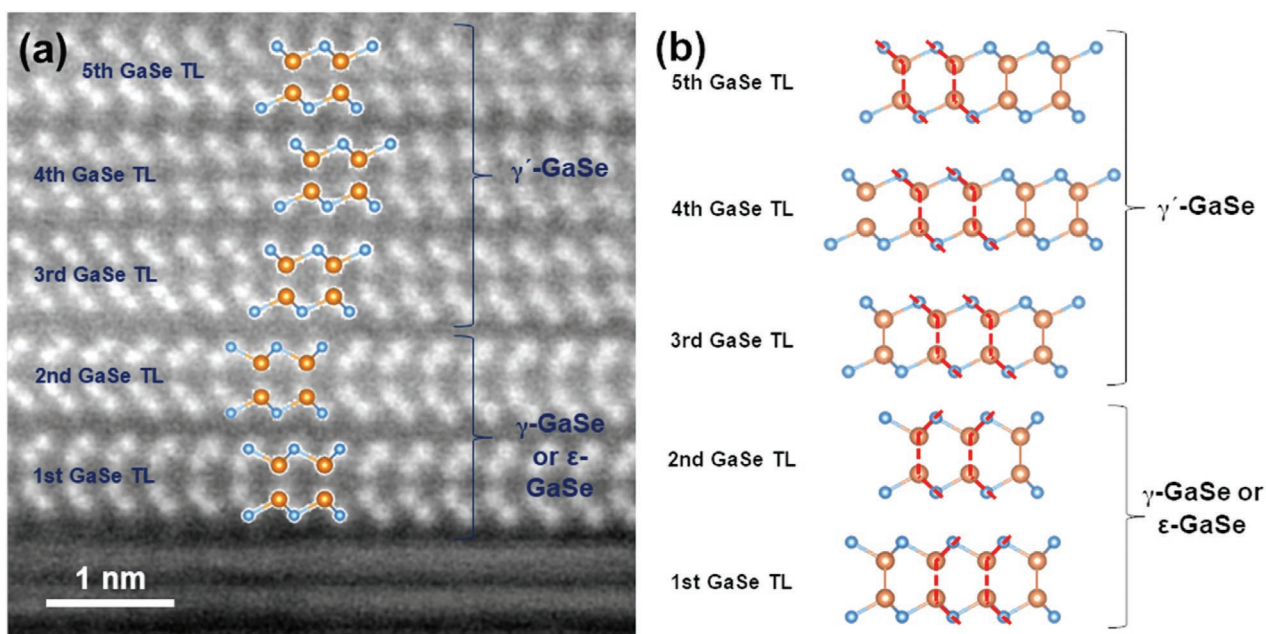
Figure 7. a) HAADF-STEM image showing the transition from a γ/ε-GaSe structure with ncs-TLs to a γ'-GaSe structure with cs-TLs. b) Atomic model of the various polymorphs and the stacking sequences observed in (a).
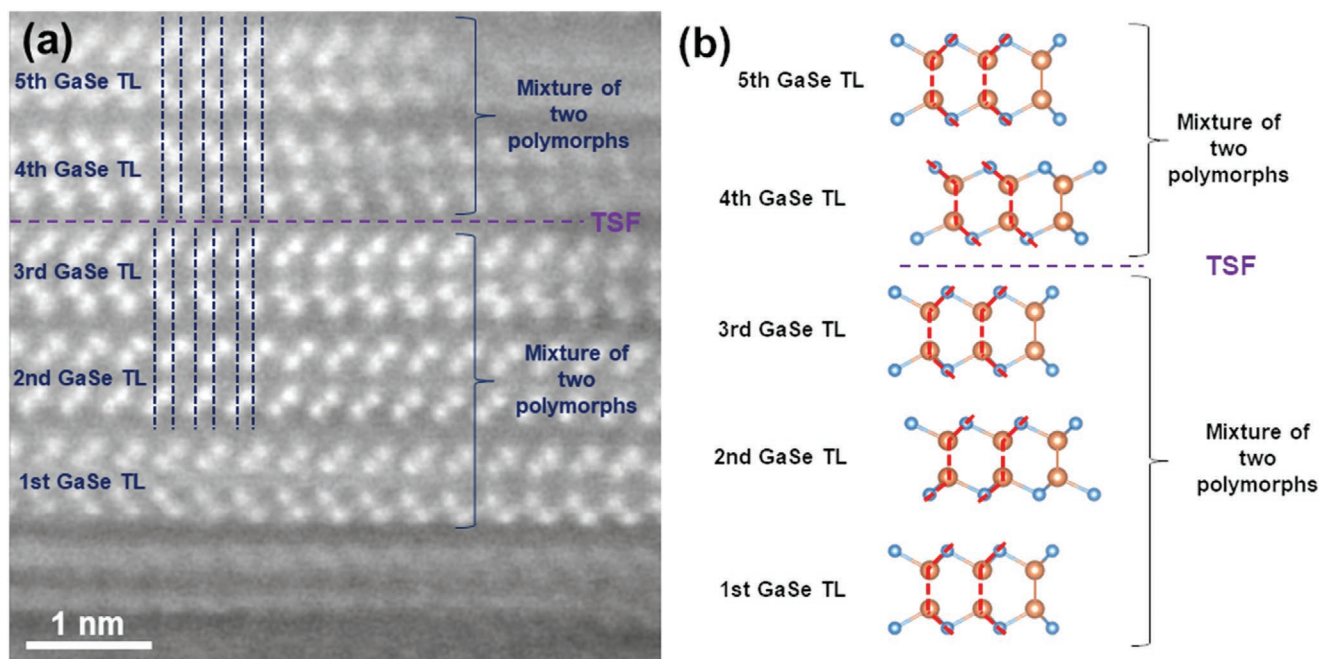
Figure 8. a) HAADF-STEM image of alternating TLs of GaSe with regular ncs-TLs and new cs-TLs. The TSF between the 3rd and 4th GaSe TLs is marked by a purple dotted line. The dark blue dashed lines represent the TSF between TLs. b) Atomic model of the polymorphs and stacking sequence shown in (a).

a two atom columns (shown within the dashed rectangle black box in Figure S5, Supporting Information), which is located at the interface between two mirror TLs.

3. Conclusion

In conclusion, we have grown GaSe films on Si and c-sapphire substrates using MBE. A good alignment between the TLs along the c-axis and several stacking orders were found, resulting in the presence of different polytypes. Using aberration-corrected STEM, we identified a new polymorph, consisting of centrosymmetric GaSe TL (point group D_{3d}), in contrast to the well-known non-centrosymmetric GaSe TL (point group D_{3h}). The new polymorph exhibits a γ-type stacking and therefore we named it γ'-GaSe. We also identified regions where the ncs-TL alternates with the new cs-TL polymorph in a layer-by-layer fashion. Furthermore, we identified defects in the films, such as layers rotation/twisting, quasi-van der Waals gap, γ phase with a rotation of one TL of 60°, and TSFs.

Although very recently, the cs-TL polymorph has been proposed for GaSe by ab-initio calculations,[32] and the novel cs-TL polymorph has been predicted for InSe,[31] this is the first time that these structures are systematically observed on different substrates and far from the interface with the substrate. The stability of the γ'-GaSe is verified by DFT calculations, which also generated its band structure and bandgap value. Our results establish MBE as a viable path to synthesize these new centrosymmetric polymorphs of PTMC, which are predicted to exhibit enhanced optoelectronic properties.

4. Experimental Section

Van der Waals Epitaxy Growth of GaSe Films: The growth was performed in an EVO-50 MBE system (Omicron Nanotechnology GmbH). Galium (6N) was evaporated from a Knudsen cell and selenium (5 N) from a valved cracker cell. The Se was evaporated from a reservoir maintained at 285 °C, while the flux was controlled by a valve with an adjustable aperture ranging from 0 to 8 mm. Before entering the growth chamber, larger selenium molecules were cracked by the cracker stage kept at 900 °C. The stand-by base pressure of the MBE system was 2.6×10^{-10} mbar and during the growth, when the Se valve was open, the pressure increases to 10^{-8} to 10^{-7} mbar. All growth processes were observed by RHEED (Staib Instruments), which was operated at 15 kV. Epi-ready single-side polished 2-inch c-sapphire (0001) with a specified and confirmed roughness of ≈0.2 nm and epi-ready boron-doped p$^+$-Si (111) substrates were used, each substrate was annealed inside the growth chamber for 30 min at 950–1000 °C just before the growth. In the case of silicon substrates, the native oxide layer was desorbed and a 7×7 reconstruction observed in the RHEED diffraction pattern. The gallium cell temperature was set to 890 °C, to obtain growth rates of 90 nm h^{-1} which was equivalent to ≈1 TL each 45 s. The Se valve aperture was kept at 1.15 mm.

Characterization Methods: Cross-sectional transmission electron microscopy (TEM) specimen preparation was carried out by focused ion beam (FIB; Ga$^+$ ions), using a FEI Helios NanoLab 450S Dual Beam Focused Ion Beam with UHREM FEG-SEM. For the transmission electron microscopy (TEM) lamella preparation a layer of Pt was deposited to protect the sample from Ga-ion implantation and damage. The sample was thinned to near electron transparency with a 30 kV ion beam and subsequently polished with a 5 kV ion beam to remove the amorphous surface layer, which resulted from the higher energy milling.

The structures of the vdW epitaxial GaSe crystals were investigated using HAADF-STEM imaging, which was performed using an aberration-corrected FEI Titan Cubed Themis 60–300 kV with an X-FEG electron source operating at 200 kV. The HAADF-STEM imaging was performed using a probe convergence semiangle of 21 mrad, the inner and outer

collection angles used for HAADF were 50.5 and 200 mrad, respectively. The structural models of GaSe were built using Vesta software.[40]

The surface morphology of the samples was examined by AFM (Bruker Icon). Due to the oxidation of GaSe in ambient conditions, AFM scans were performed immediately after the growth. The measurements were taken in tapping-mode using PPP-NCH (NanosensorsTM) cantilevers with a nominal tip radius of <20 nm, force constant of 42 N m^{-1}, and ≈265 kHz resonance frequency.

Raman spectroscopy was measured at room temperature in a WITec alpha300 R confocal microscope, using a 50× objective lens, and a solid-sate 532 nm excitation laser with average power below 1 mW to prevent local overheating and oxidation. XRD measurements were performed in a PANalytical Xpert PRO MRD diffractometer with 5-axis cradle, standard Bragg–Brentano (BB) geometry, Cu anode X-ray tube operated at 45 kV accelerating voltage, and 40 mA filament current to generate X-rays (Cu K-alpha). Soller and collimation 0.5″ slits were used in the source side and detection using Soller slits and CCD detector (PiXcel) inline (1D) model. The gracing-incidence XRD (GIIXRD) (and φ-scan) was done in similar configuration (BB), but with the addition of a Goebel mirror in the source side and using open-detector for detection.

Theoretical Calculations: The ab-initio calculations had been performed using density perturbation theory (DFT) within the local-density approximation (LDA) as implemented in Quantum Espresso using norm-conserving pseudopotentials.[41,42] The vdW interaction was accounted with the semiempirical Grimme's DFT-3 method.[43] The authors had optimized lattice parameters and atomic positions until forces in each atom were smaller than 0.01 eV Å^{-1}. For all systems, the basis-set cutoff energy was 120 Ry and the sampling of the Brillouin zone was a $12 \times 12 \times 5$ k-grid. The dispersion of the bands along the k_z direction was rather flat and it is not shown in Figure 5. The optimization of the lattice parameters gives small differences. For the γ phase the authors had found $a = 3.80$ and $c = 23.66$ Å. For the γ phase the lattice parameters were $a = 3.81$ and $c = 23.57$ Å. The calculations of the phonon frequencies and the Raman tensor were performed within the formalism of density-functional perturbation theory and the method of Lazzeri and Mauri.[44]

Supporting Information

Supporting Information is available from the Wiley Online Library or from the author.

Conflict of Interest

The authors declare no conflict of interest.

Data Availability Statement

The data that support the findings of this study are available from the corresponding author upon reasonable request.

[1] K. S. Novoselov, A. Mishchenko, A. Carvalho, A. H. Castro Neto, *Science* **2016**, *353*, aac9439.
[2] Y. Ma, Y. Dai, M. Guo, L. Yu, B. Huang, *Phys. Chem. Chem. Phys.* **2013**, *15*, 7098.
[3] M. W. Chen, H. K. Kim, D. Ovchinnikov, A. Kuc, T. Heine, O. Renault, A. Kis, *npj 2D Mater. Appl.* **2018**, *2*, 2.
[4] X. Li, M. W. Lin, A. A. Puretzky, J. C. Idrobo, C. Ma, M. Chi, M. Yoon, C. M. Rouleau, I. I. Kravchenko, D. B. Geohegan, K. Xiao, *Sci. Rep.* **2014**, *4*, 5497.
[5] D. V. Rybkovskiy, A. V. Osadchy, E. D. Obraztsova, *Phys. Rev. B: Condens. Matter Mater. Phys.* **2014**, *90*, 235302.
[6] D. Wickramaratne, F. Zahid, R. K. Lake, *J. Appl. Phys.* **2015**, *118*, 075101.
[7] H. C. Koo, S. B. Kim, H. Kim, T. E. Park, J. W. Choi, K. W. Kim, G. Go, J. H. Oh, D. K. Lee, E. S. Park, I. S. Hong, K. J. Lee, *Adv. Mater.* **2020**, *32*, 2002117.
[8] L. Seixas, A. S. Rodin, A. Carvalho, A. H. Castro Neto, *Phys. Rev. Lett.* **2016**, *116*, 206803.
[9] T. Cao, Z. Li, S. G. Louie, *Phys. Rev. Lett.* **2015**, *114*, 236602.
[10] D. A. Bandurin, A. V. Tyurnina, G. L. Yu, A. Mishchenko, V. Zólyomi, S. V. Morozov, R. K. Kumar, R. V. Gorbachev, Z. R. Kudrynskyi, S. Pezzini, Z. D. Kovalyuk, U. Zeitler, K. S. Novoselov, A. Patanè, L. Eaves, I. V. Grigorieva, V. I. Fal'ko, A. K. Geim, Y. Cao, *Nat. Nanotechnol.* **2017**, *12*, 223.
[11] M. Brotons-Gisbert, D. Andres-Penares, J. Suh, F. Hidalgo, R. Abargues, P. J. Rodríguez-Cantó, A. Segura, A. Cros, G. Tobias, E. Canadell, P. Ordejón, J. Wu, J. P. Martínez-Pastor, J. F. Sánchez-Royo, *Nano Lett.* **2016**, *16*, 3221.
[12] D. J. Terry, V. Zólyomi, M. Hamer, A. V. Tyurnina, D. G. Hopkinson, A. M. Rakowski, S. J. Magorrian, N. Clark, Y. M. Andreev, O. Kazakova, K. Novoselov, S. J. Haigh, V. I. Fal'Ko, R. Gorbachev, *2D Mater.* **2018**, *5*, 041009.
[13] C. H. Lee, S. Krishnamoorthy, D. J. O'Hara, M. R. Brenner, J. M. Johnson, J. S. Jamison, R. C. Myers, R. K. Kawakami, J. Hwang, S. Rajan, *J. Appl. Phys.* **2017**, *121*, 094302.
[14] N. C. Fernelius, *Prog. Cryst. Growth Charact. Mater.* **1994**, *28*, 275.
[15] F. H. Herbstein, *Cryst. Growth Des.* **2004**, *4*, 1419.
[16] H. Bergeron, D. Lebedev, M. C. Hersam, *Chem. Rev.* **2021**, *121*, 2713.
[17] J. Srour, M. Badawi, F. El Haj Hassan, A. Postnikov, *J. Chem. Phys.* **2018**, *149*, 054106.
[18] Y. Tang, W. Xie, K. C. Mandal, J. A. McGuire, C. W. Lai, *Phys. Rev. B: Condens. Matter Mater. Phys.* **2015**, *91*, 195429.
[19] A. Gouskov, J. Camassel, L. Gouskov, *Prog. Cryst. Growth Charact.* **1982**, *5*, 323.
[20] X. Li, L. Basile, M. Yoon, C. Ma, A. A. Puretzky, J. Lee, J. C. Idrobo, M. Chi, C. M. Rouleau, D. B. Geohegan, K. Xiao, *Angew. Chem., Int. Ed.* **2015**, *54*, 2712.

ADVANCED
SCIENCE NEWS
www.advancedsciencenews.com

ADVANCED
FUNCTIONAL
MATERIALS
www.afm-journal.de

[21] K. Ueno, N. Takeda, K. Sasaki, A. Koma, *Appl. Surf. Sci.* **1997**, *113*, 38.

[22] L. T. Vinh, M. Eddrief, C. Sébenne, A. Sacuto, M. Balkanski, *J. Cryst. Growth* **1994**, *135*, 1.

[23] A. Koëbel, Y. Zheng, J. F. Pétroff, M. Eddrief, L. T. Vinh, C. Sébenne, *J. Cryst. Growth* **1995**, *154*, 269.

[24] S. V. Sorokin, P. S. Avdienko, I. V. Sedova, D. A. Kirilenko, M. A. Yagovkina, A. N. Smirnov, V. Y. Davydov, S. V. Ivanov, *Semiconductors* **2019**, *53*, 1131.

[25] Z. R. Dai, S. R. Chegwidden, L. E. Rumaner, F. S. Ohuchi, *J. Appl. Phys.* **1999**, *85*, 2603.

[26] C. De Blasi, D. Manno, A. Rizzo, *Nuovo Cimento D* **1989**, *11*, 1145.

[27] S. V. Sorokin, P. S. Avdienko, I. V. Sedova, D. A. Kirilenko, V. Y. Davydov, O. S. Komkov, D. D. Firsov, S. V. Ivanov, *Materials* **2020**, *13*, 3447.

[28] S. J. Magorrian, V. Zólyomi, N. D. Drummond, *Phys. Rev. B: Condens. Matter Mater. Phys.* **2021**, *103*, 94118.

[29] G. Eda, T. Fujita, H. Yamaguchi, D. Voiry, M. Chen, M. Chhowalla, *ACS Nano* **2012**, *6*, 7311.

[30] M. Chhowalla, H. S. Shin, G. Eda, L. J. Li, K. P. Loh, H. Zhang, *Nat. Chem.* **2013**, *5*, 263.

[31] Y. Sun, Y. Li, T. Li, K. Biswas, A. Patanè, L. Zhang, *Adv. Funct. Mater.* **2020**, *30*, 2001920.

[32] H. Nitta, T. Yonezawa, A. Fleurence, Y. Yamada-Takamura, T. Ozaki, *Phys. Rev. B: Condens. Matter Mater. Phys.* **2020**, *102*, 235407.

[33] X. Li, L. Basile, B. Huang, C. Ma, J. Lee, I. V. Vlassiouk, A. A. Puretzky, M. W. Lin, M. Yoon, M. Chi, J. C. Idrobo, C. M. Rouleau, B. G. Sumpter, D. B. Geohegan, K. Xiao, *ACS Nano* **2015**, *9*, 8078.

[34] A. Koma, *Thin Solid Films* **1992**, *216*, 72.

[35] R. Fritsche, E. Wisotzki, A. B. M. O. Islam, A. Thissen, A. Klein, W. Jaegermann, R. Rudolph, D. Tonti, C. Pettenkofer, *Appl. Phys. Lett.* **2002**, *80*, 1388.

[36] A. M. Mio, P. M. Konze, A. Meledin, M. Küpers, M. Pohlmann, M. Kaminski, R. Dronskowski, J. Mayer, M. Wuttig, *Adv. Funct. Mater.* **2019**, *29*, 1902332.

[37] J. F. Sánchez-Royo, G. Muñoz-Matutano, M. Brotons-Gisbert, J. P. Martínez-Pastor, A. Segura, A. Cantarero, R. Mata, J. Canet-Ferrer, G. Tobias, E. Canadell, J. Marqués-Hueso, B. D. Gerardot, *Nano Res.* **2014**, *7*, 1556.

[38] G. Onida, L. Reining, A. Rubio, *Rev. Mod. Phys.* **2002**, *74*, 601.

[39] T. Yonezawa, T. Murakami, K. Higashimine, A. Fleurence, Y. Oshima, Y. Yamada-Takamura, *Surf. Interface Anal.* **2019**, *51*, 95.

[40] K. Momma, F. Izumi, *J. Appl. Crystallogr.* **2011**, *44*, 1272.

[41] P. Giannozzi, S. Baroni, N. Bonini, M. Calandra, R. Car, C. Cavazzoni, D. Ceresoli, G. L. Chiarotti, M. Cococcioni, I. Dabo, A. Dal Corso, S. De Gironcoli, S. Fabris, G. Fratesi, R. Gebauer, U. Gerstmann, C. Gougoussis, A. Kokalj, M. Lazzeri, L. Martin-Samos, N. Marzari, F. Mauri, R. Mazzarello, S. Paolini, A. Pasquarello, L. Paulatto, C. Sbraccia, S. Scandolo, G. Sclauzero, A. P. Seitsonen, A. Smogunov, P. Umari, R. M. Wentzcovitch, *J. Phys.: Condens. Matter* **2009**, *21*, 395502.

[42] P. Giannozzi, O. Andreussi, T. Brumme, O. Bunau, M. Buongiorno Nardelli, M. Calandra, R. Car, C. Cavazzoni, D. Ceresoli, M. Cococcioni, N. Colonna, I. Carnimeo, A. Dal Corso, S. De Gironcoli, P. Delugas, R. A. Distasio, A. Ferretti, A. Floris, G. Fratesi, G. Fugallo, R. Gebauer, U. Gerstmann, F. Giustino, T. Gorni, J. Jia, M. Kawamura, H. Y. Ko, A. Kokalj, E. Kücükbenli, M. Lazzeri, M. Marsili, N. Marzari, F. Mauri, N. L. Nguyen, H. V. Nguyen, A. Otero-De-La-Roza, L. Paulatto, S. Poncé, D. Rocca, R. Sabatini, B. Santra, M. Schlipf, A. P. Seitsonen, A. Smogunov, I. Timrov, T. Thonhauser, P. Umari, N. Vast, X. Wu, S. Baroni, *J. Phys.: Condens. Matter* **2017**, *29*, 465901.

[43] S. Grimme, J. Antony, S. Ehrlich, H. Krieg, *J. Chem. Phys.* **2010**, *132*, 154104.

[44] M. Lazzeri, F. Mauri, *Phys. Rev. Lett.* **2003**, *90*, 4.